VOL. 11, NO. 19, OCTOBER 2016 ISSN 1819-6608
ARPN Journal of Engineering and Applied Sciences

www.arpnjournals.com

ANALYSIS OF MARINE MAGNETIC DATA IN THE STUDY OF FAULTS AND BASEMENT IN PENYU BASIN OFFSHORE PENINSULAR MALAYSIA

Umar Hamzah, Abdul Rahim Samsudin and Nadiah Hanim Shafie
Geology Programme, PPSSSA, Faculty of Science and Technology, National University of Malaysia, Malaysia
E-Mail: umar@ukm.edu.com

ABSTRACT

In this paper, attempt has been made to detect the basement depth underlying the Tertiary deposit and the structural lineaments within the Penyu basin by applying 3D Euler deconvolution technique to the magnetic field data. Basement depth and the structural trend estimation were done by Oasis Montaj computer software using window size (W) of 20 corresponding to about 20 X 20 km width of the magnetic data station distribution. Structural Index parameter (SI) of 0, for sheet body magnetic source was used for the faults determination. Results obtained were compared with seismic line across the study area. Basement depths from 3D Euler analysis are ranging from 3-6 km comparable to depths interpreted from seismic data. 2D sections developed of 3D Euler deconvolution map along N-S clearly displayed the arrangement of magnetic sources at depths forming normal faults with flower structures as well as the horst and graben features within the faults. The faults strike approximately in the E-W direction and dip towards the north and south. The faults positions in the seismic sections are well correlated when superimposed with the magnetic lineaments corresponding to faults obtained by Euler deconvolution.

Keywords: magnetic anomaly, basement depth, 3D Euler deconvolution, penyu basin.

1. INTRODUCTION

The importance of magnetic survey in the determination of structural features such as faults and sheared zones which always related to mineral exploration has been tremendous and reported over the past few decades (Opara *et al.* 2015, Waswa *et al.* 2015 and Santos *et al.* 2015). These structural discontinuities either located in sedimentary basin or in the basement rock underlying it can easily be mapped by spectral analysis or 3D Euler deconvolution (Salem *et al.* 2000, Reid *et al.* 1990). In the case of Euler Deconvolution technique, the estimation of structural index and depth to the source is the main task of many popular methods used to analyze potential field data (Floria *et al.* 2014). Thickness of sedimentary basin deposit overlying the crustal material and depth of Mohorovic surface were estimated by spectral analysis technique of magnetic data as reported in Hassan *et al* 2015. Edge enhancement in potential-field data helps geological interpretation, where the lineaments on the potential-field frequently indicate subsurface faults, contacts, and other tectonic features (Sun *et al.* 2016, Arisoy&Dikmen 2015; Cooper, 2014).

Magnetic survey is also considered as very potential in detecting the subsurface structural geology such as in estimating depth of basement (Kivior *et al.* 2013), faults, folds and dykes. By integrating with seismic data, the magnetic interpretation will be much promising especially in determining the subsurface rock stratigraphy. Wu *et al* (2003) used varying magnet magnetism for different rock types to identify rock distribution patterns and correlating them with age and fold structure in mountain range. Fowler (2005) explained that the magnetic anomaly variation depends on the location of regional latitude. The positive value of earth crust magnetism in the north becomes negative if it is changed to the South pole due to the reversal of the magnetic field. Almadar *et al.* (2009) shows that the Total Horizontal Derivative value can be used to determine the subsurface geological structures such as faults and igneus intrusion.

In this study, magnetic data of 100 m spacing measured at a total of 2450 stations in block P308A of Penyu basin offshore Peninsular Malaysia supplied by Petronas were used for interpretation. Figure-1 shows the location of Penyu basin off Pahang offshore in the eastern part of peninsular Malaysia. Total area of Penyu basin is about 14, 000 km^2 with sediment thickness of about 5000 m. Out of this total area, data coverage was within about 2000 km^2 from latitude of 405000 to 380000 and longitude of 440000 to 480000. The main aim of this study was to map the basement depth and related major faults trends along the basement as well as in the sediment succession in cross section. These objectives were achieved by the application of 3D Euler deconvolution technique to the available magnetic data. 2.5D forward modelling of selected magnetic profiles was undertaken to verify and validate the interpreted basement configuration.

Penyu basin is one of three main basin located in the South China Sea beside Malay and East Natuna basins. Penyu basin shallow marine Oligocene sediment is deposited on top of Pahang platform and is believed to be connected to the East Natuna basin (Mazlan *et al.* 1997). MazlanMadon (1995) also stated that this Penyu basin consists of several graben and half-graben such as Kuantan, Pekan, Rumbia and Merchong grabens divided by major faults.

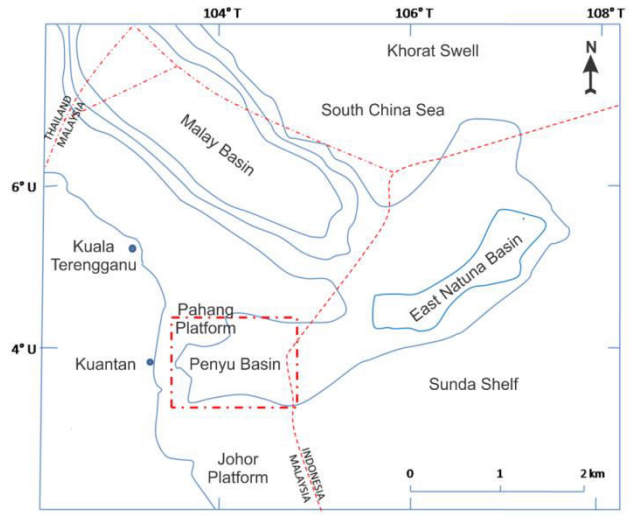

Figure-1. Map of study of Penyu basin located east of Peninsular Malaysia.

Penyu basin is situated in Sunda shelf believed to be originated in early cretaceous to early Tertiary by similar tectonic processes (Hutchison 1989). Therefore regional tectonic history of the region should be taken into account for the understanding of Penyu basin evolution. Diversified structural features in the basin may be related to compressional and extensional forces occurred during the basin formation. The collision of Australia-India plate against the Eurasian plate took place during early Palaeocene till middle to late Eocene which resulted to the subduction activity of the same plate below the Sunda arc parallel to Sumatra (Packham, 1993). This subduction event has pressurized and uplifted the Sunda shelf to form domal features in the region. The huge compression has produced several week zones or faults along EW and NW-SE orientations. The strong compression also sheared the faults in the right and left directions to cause opening along the rifts to form basins in the region for the sediment depositions. The subduction continued aggressively till late Oligocene causing trans-tensional movements far away from the plate boundary especially along the old faults in the old Sunda craton (Ngah *et al.* 1996). Right-lateral shearing due to subduction activity has widened the extensional faults towards the west to form grabens which served to be the site of the sediment deposition in Malay basin and other nearby basins. The grabens became continuously deepen during Oligocene till early Miocene causing sediment of about 2600m thick to be deposited in the basin. Ngah *et al.* (1996) also believed that plate repositioning took place during early Miocene till mid Miocene producing residual stress to cause sedimentary deformation in Malay, Penyu and Natuna basinsand regional unconformity.

2. METHODOLOGY

Raw data were acquired from marine survey along 100 lines of 23 km length each. A total of about 2451 measurements points were made at stations of 100m spacing. Magnetic measurement points along all survey lines with an azimuth of N355E are as shown in Figure-2. All data reductions were carried out by PETRONAS and the resulting total magnetic intensity (TMI) values were used in this study for geological interpretation by OASIS MONTAJ GEOSOFT computer software. This software was used to generate the total magnetic intensity map as well as to filter them into producing the reduction to the equator (RTE) values, total horizontal derivative (THD) and 3D Euler Deconvolution maps. The same software may also be used for modelling and inversion of the subsurface bodies.

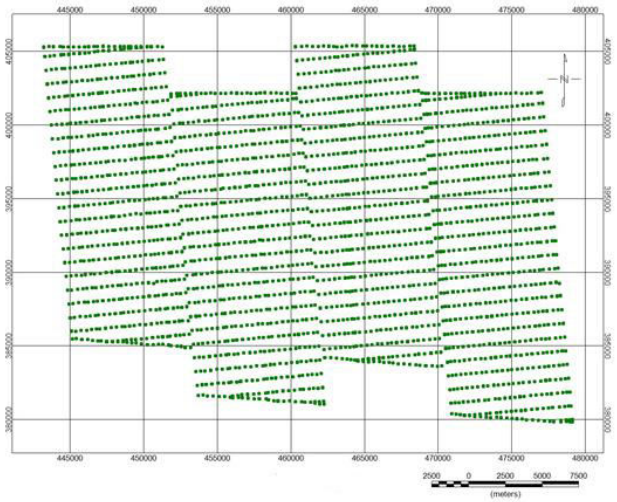

Figure-2. Location of marine magnetic survey stations.

Filtering for RTE was carried out for converting the total magnetic intensity into magnetic intensity with 90° slope. Magnetic anomaly at low latitude becomes dipoles which are not equivalent to the source of anomaly. Reduction to equator will change the magnetic intensity of the source body into monopole to enhance the interpretation. Filtering is made by assuming the induced magnetic field is parallel to the earth magnetic field and hence equivalent to the remnant magnetization. The formula for reduction to equator is as given below:

$$L(\theta) = \frac{1}{(\sin(I_a)+Ikos(I)-kos(D-\theta))^2} \quad (1)$$

Where I_a is a slope for magnitude correction, I is the geomagnetic slope and D is the geomagnetic inclination. Reduction to the pole was also carried out in this survey since according to Wu (2004), it has to be carried out for any survey located above 30° latitude while reduction to equator has to be carried for survey area below than 25° latitude.

Total horizontal derivative (THD) technique measures the rate of gravity field changes along X and Y directions. This method used gravity data to detect density boundary by enhancing the high anomaly as observed in areas of faults, dykes and lineaments. (Cordell 1979, Almadar *et al.* 2009). The formula used in deriving the THD is given as;

$$\text{THD} = \sqrt{\left[\frac{\partial T}{\partial x}\right]^2 + \left[\frac{\partial T}{\partial y}\right]^2} \quad (2)$$

Where T is the anomaly$\frac{dT^2}{dx}$ is the anomaly along $x = 0^{\circ}$ and $\frac{dT^2}{dy}$ is the anomaly along $y = 90^{\circ}$direction.

3D Euler deconvolution is used to interpret the gravity and magnetic data especially in detecting depths and positions of the subsurface source anomalies in the study area (Reid, 1995) by applying MAGMAP 2D Fast Fourier Transform. Information rendered by the filtering includes coordinates of the subsurface structural along X, Y and Z as calculated by the equation given below through Oasis Montaj software;

$$(x - x_1)\frac{\delta g}{\delta x} + (y - y_1)\frac{\delta g}{\delta y} + (z - z_1)\frac{\delta g}{\delta z} = N(B - g) \quad (3)$$

Where g is the gravity anomaly found at (x, y, z) representing a body at (x_1, y_1, z_1). B referred to regional magnetic value at (x, y) and N is a constant representing structural index (SI). Depth and location of magnetic source can be determined by using Euler deconvolution function by proper selection of several parameters such as by choosing the correct structural index between 0-3 and also by adjusting the percentage depth tolerance as well as the window size. There are suitable values for SI representing several magnetic and gravity models can be used in the 3D Euler deconvolution as shown in Table 1 (Reid *et al*. 2012). In the case of fault and structural modelling the most suitable value for SI is 0 for both gravity and magnet surveys.

Table-1. Structural index of Euler deconvolution.

Model	Gravity SI	Magnetic SI
Contact of infinite depth extend, thin sheet edge		0
Thin sheet edge, thin sill, dyke	0	1
Line, cylinder, thin bed fault	1	2
Point, sphere	2	3

Possible depth estimate for subsurface geological formation in any study area is obtained by adjusting the window size, depth tolerance and structural index parameters. The resulting depth and structural pattern are then compared with the regional geology of the study area. Testing parameters correlated well with geological information either from borehole or seismic section will be selected as the final parameters. Basically, the best window used in this study is 8-11 with depth tolerance of 10 and the most suitable structural index of 0-1 for fault contact determination.

3. RESULTS AND DISCUSSIONS

The total magnetic intensity values calculated were then reduced to equator (RTE) and the values were used to generate the map as shown in Figure-3. Basically, the intensity values range from -52.1 nT to -179.5 nT. In general a body with high magnetic susceptibility will be represented by positive anomaly value and the negative value will represent the low susceptibility body. The negative anomaly values representing the whole study area with higher susceptibility body showing higher negative anomaly may indicate the area was formed during a reversal of the earth magnetic field. The lowest magnetic intensity is found in the middle of the study area sandwiched by higher magnetic intensity in the north and south forming some kind of a depression or valley shape. The magnetic anomaly pattern can be easily interpreted as the occurrence of a horst and graben structure with faults separating them along boundaries of highs and lows magnetic intensities trending almost E-W.

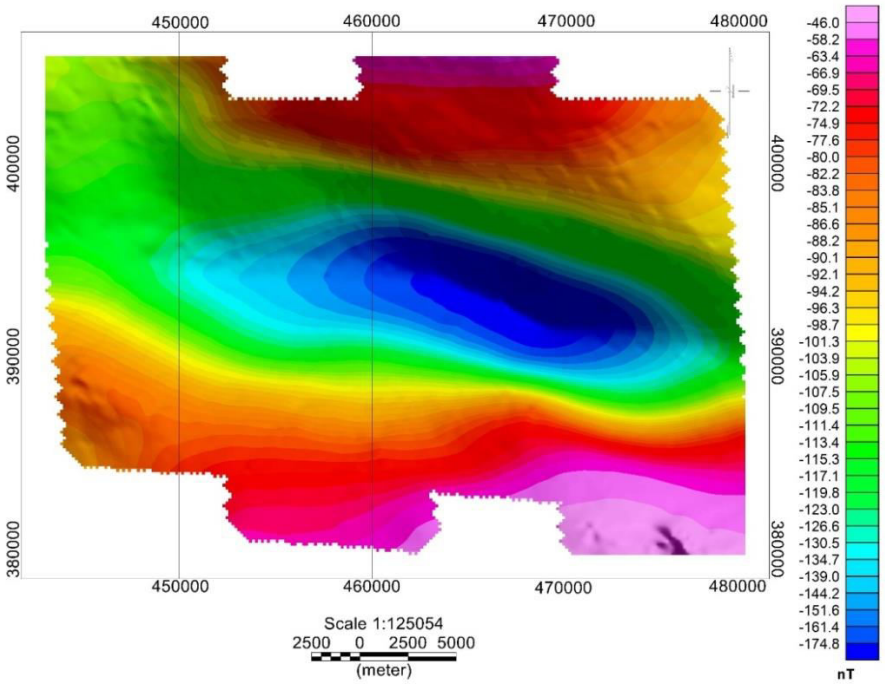

Figure-3. Contour of RTE (Reduction to equator) of the total magnetic anomalies.

Figure-4 shows the Total horizontal derivative (THD) map derived from RTE with inclination, declination and total magnetic field of -9.803°, 0.421° and 41472.4 nT respectively. The THD ranges from 6 X 10^{-4} to 71 X 10^{-4}nT. The magnetic intensity values show a trend of high in the north and south with a low value located in the middle of the study area. The elongated negative lows trends almost E-W in direction. This low magnetic zone corresponds to high granite basement flanked by higher anomalies corresponding to thicker sediment overlying the granite basement. Almost straight and slightly undulating boundaries in the northern and southern parts between high and low magnetic anomalies are correlated to faults positions forming horst and graben.

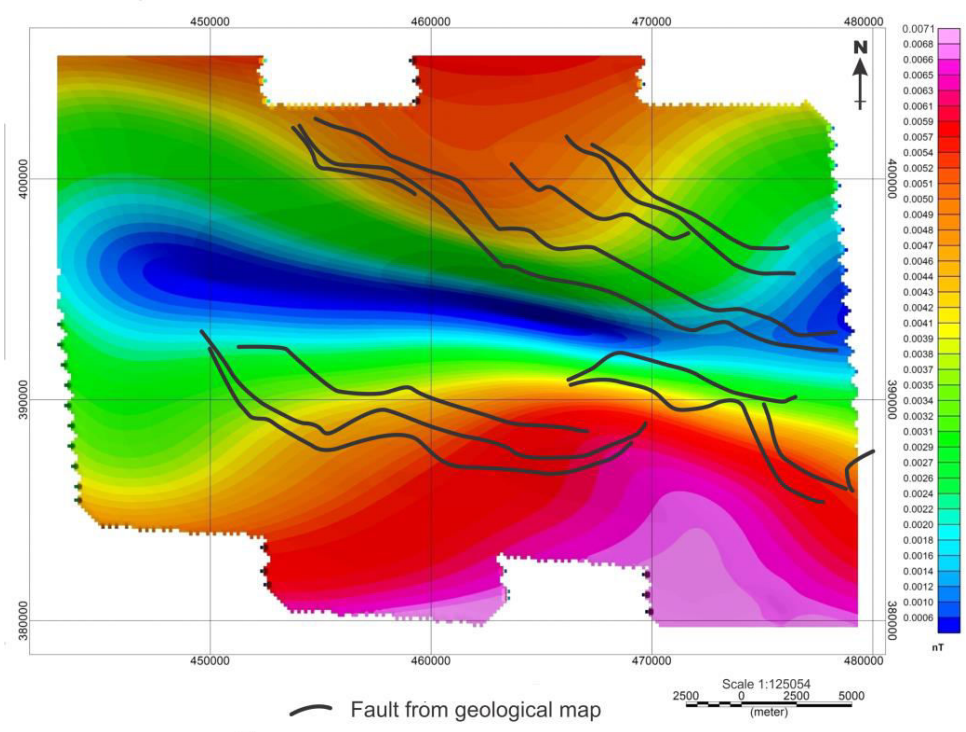

Figure-4. Total Horizontal Derivative (THD) of regional magnetic field indicating structures in the bedrock. Superimposed of the fault trends from geological information indicate faults are from shallower part.

Filtering to generate total horizontal derivative (THD) map from the RTE data was also carried out to display variation of magnetic anomaly laterally along X and Y axis. This kind of map is very suitable in exploring the presence of structural features such as shallow subsurface lineaments especially the shallow faults. Fault lineaments are always determined by locating the demarcations between high and low magnetic intensities. The fault positions need also be correlated with the major faults of the study area based on available geological map of the same area. Figure-5 shows the THD residual anomaly map with interpreted fault positions verified by structural map. The main criteria of the NW-SE fault lines are indicated by abrupt changes of the THD values from 0.0005 to 0.0198 nT. Based on Figure-5, the fault boundaries separating the high anomaly can be associated with basement high namely central high and grabens in the northern and southern parts of the study area. The Rose plot indicates the overall fault trends observed in the THD map with highest population of faults are trending towards N110-120°E. Filtering was also carried out to detect horizontal variation of magnetic anomalies for deeper zone by applying the total horizontal derivative filter to regional magnetic anomaly map. The magnetic trend is then compared with the positions of faults from a seismic study. Both faults and the magnetic anomaly are aligned along the same direction indicating faults originated from deeper zone (Figure-5).

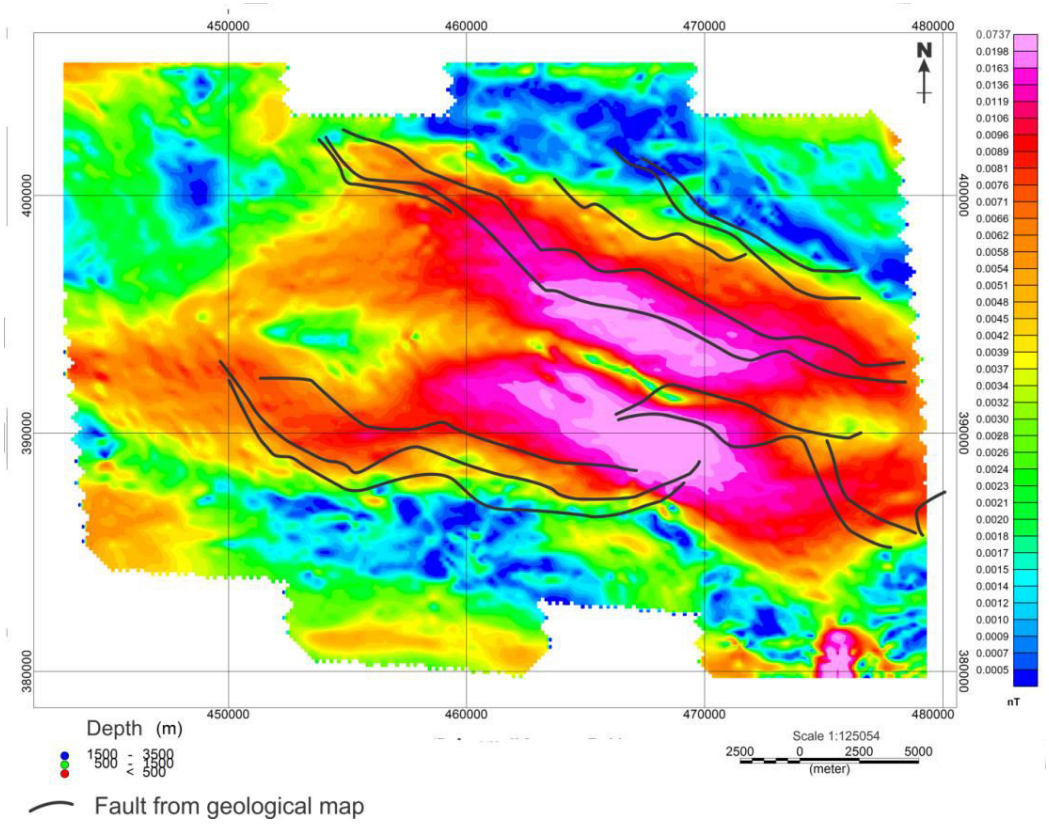

Figure-5. THD residual from RTE representing top structures below 3500m.

Total vertical derivative (TVD) maps were also derived from regional, residual and RTE magnetic anomalies purposely to investigate the vertical and deeper magnetic anomalies associated with faults in the study area. Figure-6 shows the TVD map of the regional magnetic anomaly indicating magnetic lows in the middle of the study area with values ranging from -0.0058 nT to -0.0007nT. This low zone elongates NW-SE and bordered in the north and south with magnetic highs ranging from -0.0005 to 0.0252 nT representing the cliff of deep graben towards the north and south of Penyu basin. Fault lines obtained from geology and seismic were superimposed on this map and found that these faults are perfectly matched with the southern horst-graben boundary. Only part of the faults matched with the northern horst-graben boundary indicating that the faults are of shallow zone. Figure-7 and Figure-8 show maps of TVD derived from residual and RTE data especially in calculating the magnetic shallow anomalies sources which are mostly associated with faults and any magnetic body. Both maps show almost identical NW-SE anomaly distribution and perfectly matched with the geological fault lines on top of basement rock.

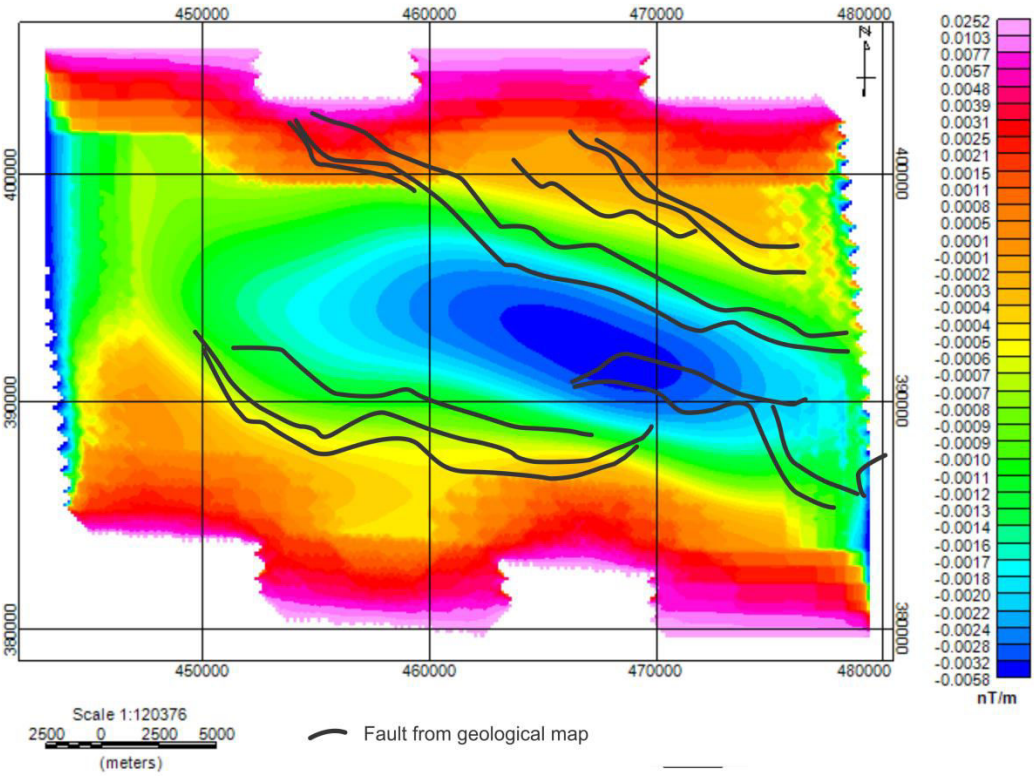

Figure-6. Total vertical derivative (TVD) of regional magnetic anomalies representing deep basement body.

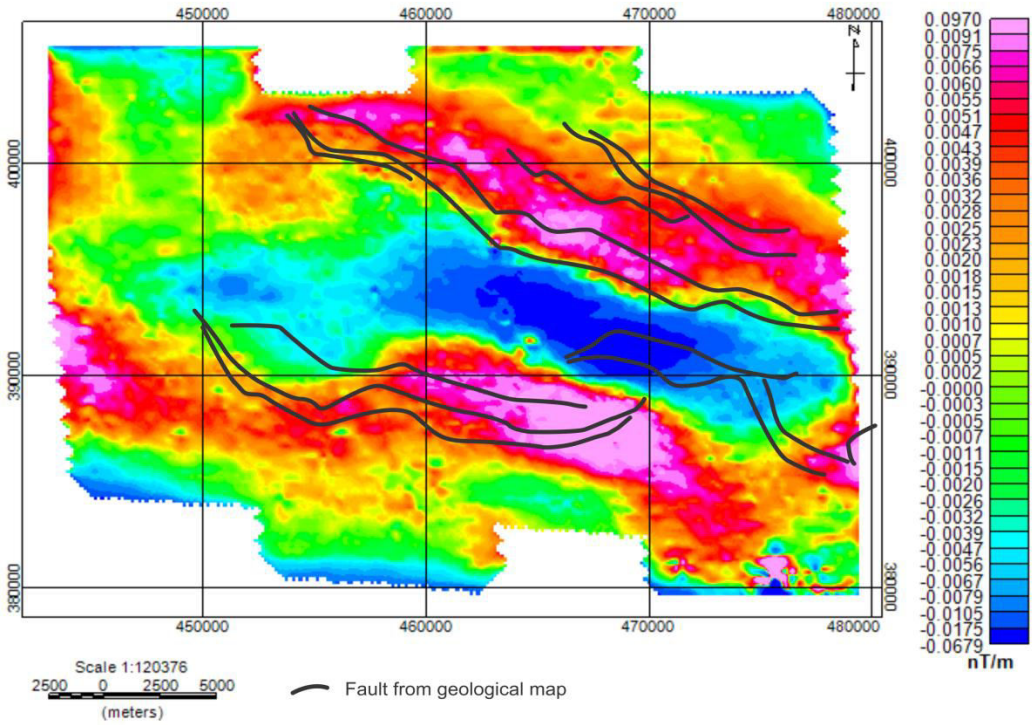

Figure-7. Total vertical derivative (TVD) of residual magnetic field representing shallow body.

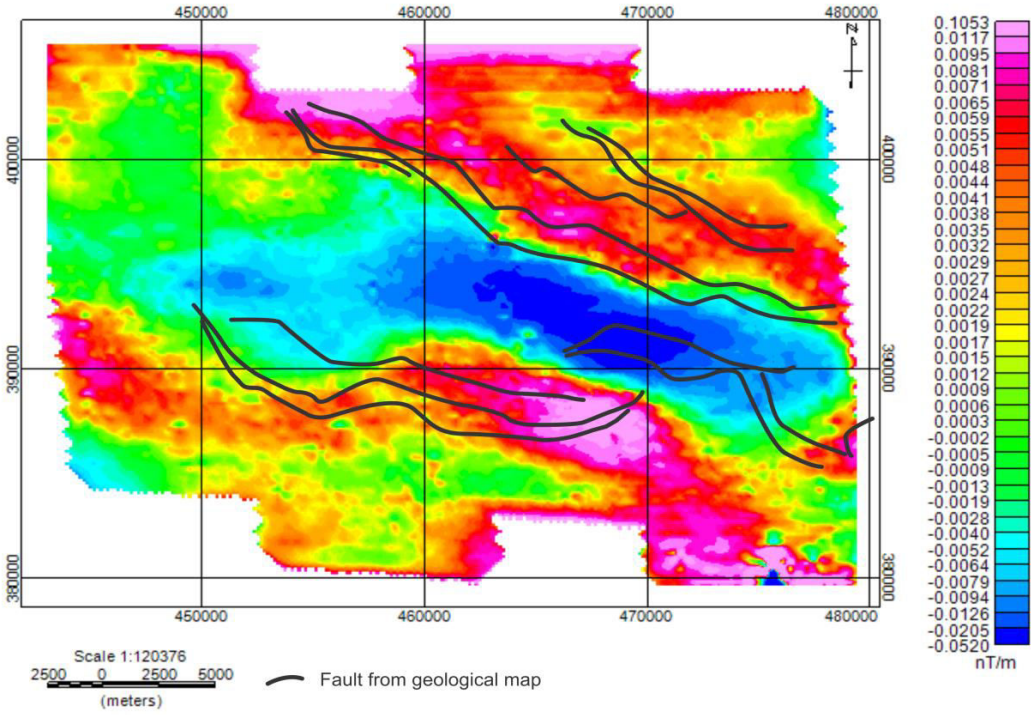

Figure-8. Total vertical derivative (TVD) map of RTE.

In addition to filtering, magnetic data were also used for 3D Euler deconvolution analysis especially for estimating each of the subsurface magnetic anomaly source depth in the study area. Maps of magnetic anomaly source depth as well as cross sections along several selected traverses of the map are generated by this 3D Euler inversion technique. Based on trial and error, the best window selected for Euler deconvolution was 11 km X 11 km cell area indicating the minimum width and length size of the data stations coverage cell for each inversion. Structural indices (SI) ranging from 0 to 3 were tested in this study for fault plane analysis especially in estimating contacts between rock types and faults in the sediment overlying the basement as well as their extensions in the basement. Figure-9 shows maps of test results using window 11 and SI form 0 to 3. Figure-9(a) represents the most suitable map (W=11 and SI=0) based on its lineaments of magnetic source depths which resemble the fault patterns of the study area as determined from seismic sections. In general, the fault depths range from 1-4 km and striking in E-W direction. Fault lines are chosen from depth points which fall along continuous or sub-continuous lineaments across the sedimentary layers or basement. Map representing the most suitable structural patterns is then compared with the geologically derived faults locations as shown in Figure-10. Highly concentrated zones of the high magnetic sources matched well with faults positions and many smaller and detail faults lineaments are observed from the Euler deconvolution map. Cross sections along 3 lines in N-S direction across the faults (A-C) of the 3D Euler map were generated for locating the faults extension below the surface (Figure-11). Prior to generating cross section from the Euler map, the fault patterns of the map were also compared with the fault patterns derived geologically and seismic data from previous study as shown in Fig. 10. Even though they are not perfectly matched, both fault trends (NW-SE) are almost identical towards the NE end and comparison could not be made in the NW zone due to unavailable geological fault data. In this regard, Euler technique detects more detail information on the existing faults of the study area especially in towards the NW part. Faults trending NE-SW were discovered in the NW end of the study area as well as a few E-W trending faults in the north zone. Cross sections along A to C clearly indicate the presence of normal faults surrounding the horst and graben structures with fault planes dipping approximately towards N-S.

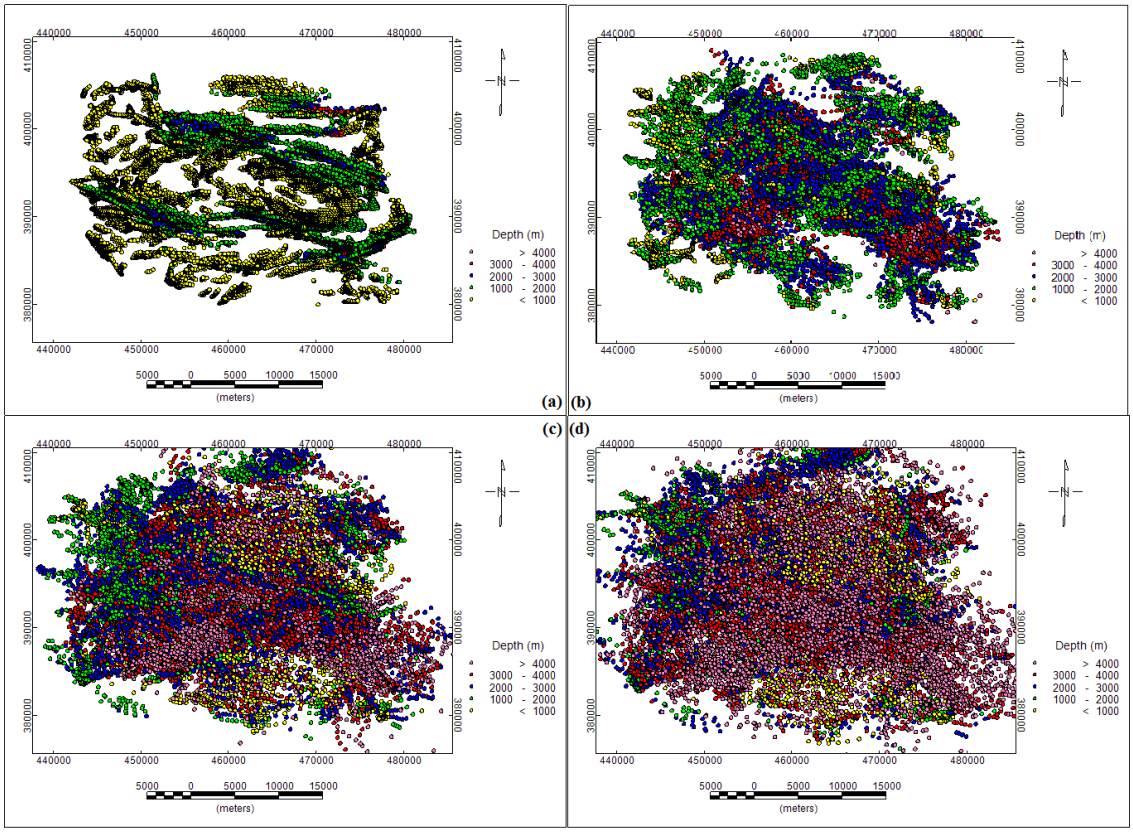

Figure-9 (a-d). Euler deconvolution maps of window 11 and different structural indices 0 to 3.

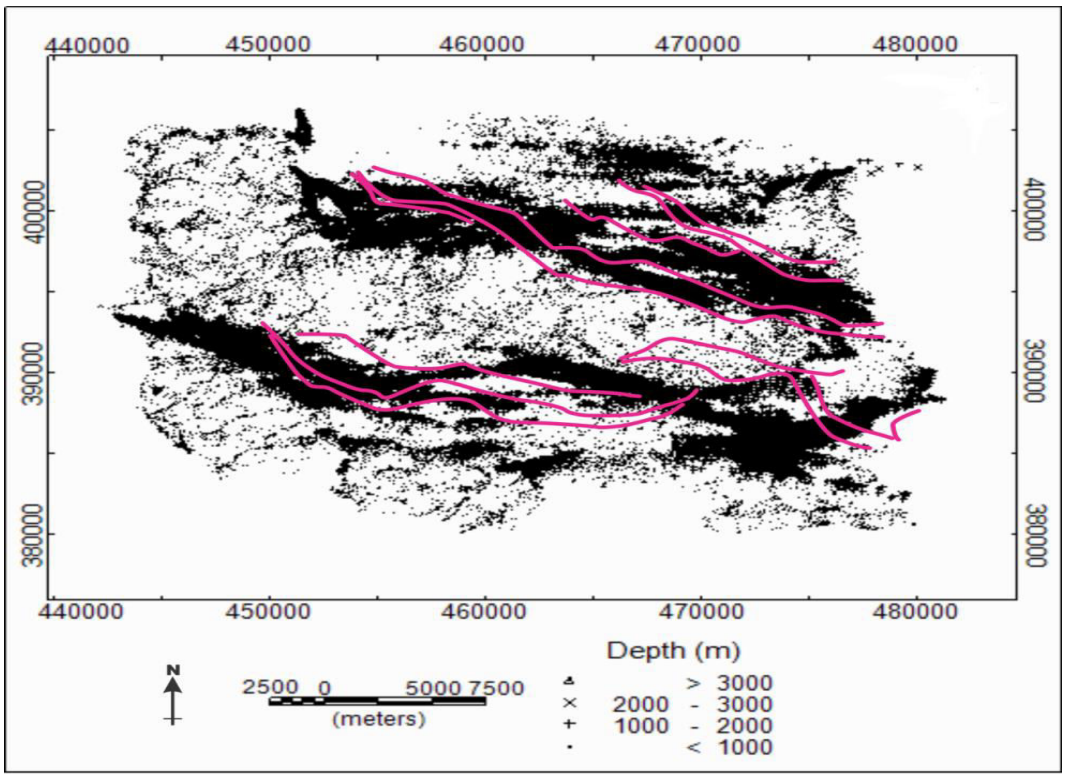

Figure-10. Euler deconvolution map of W=11 and SI=0 indicating magnetic source anomalies at different depths. Fault trends of geological study are overlapped for comparison.

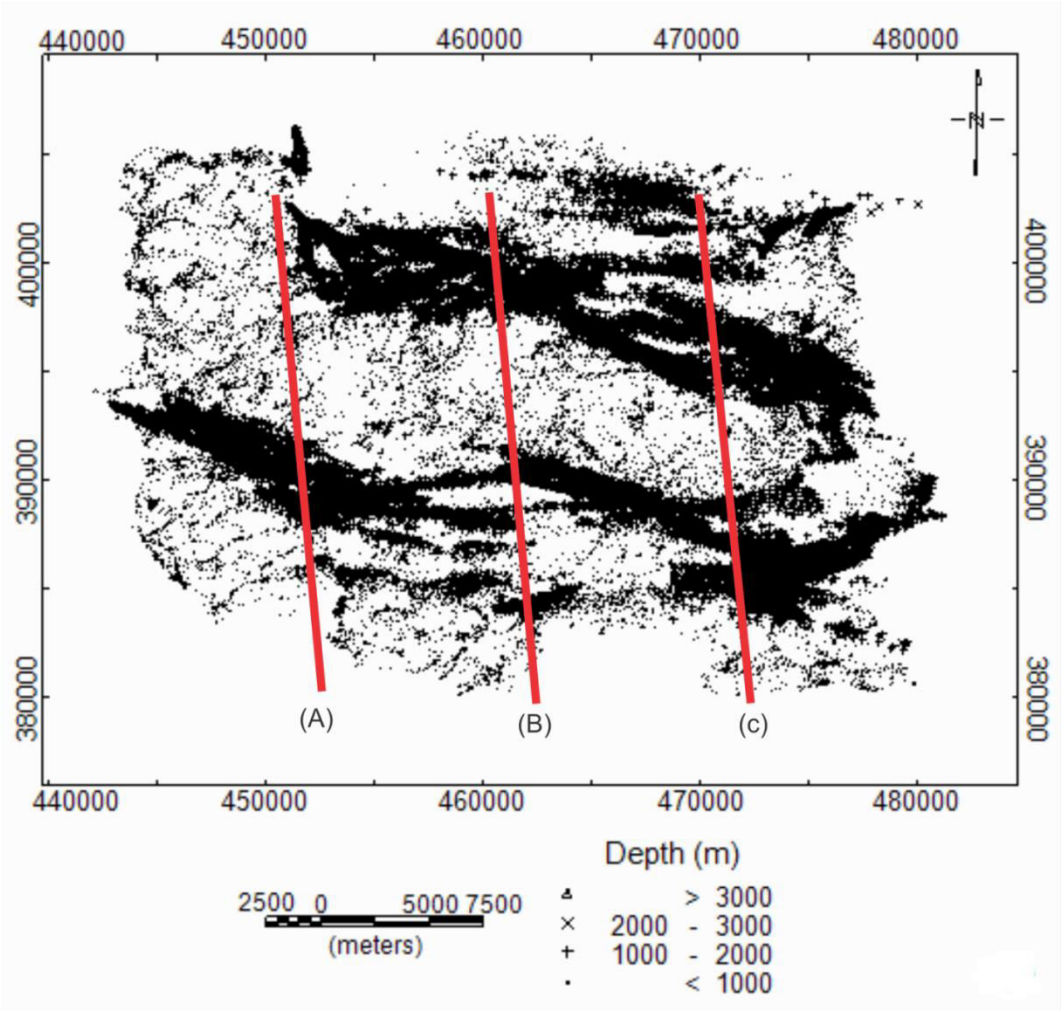

Figure-11. Positions of lines in generating cross sections of Euler anomalies for comparison with seismic.

A 25 km long seismic section of line A (Figure-12a) was interpreted and the resulting faults and basement are as shown in Figure-12(b). A big half-graben located at km 13 was observed together with another neighbouring smaller faults trending east-west in the seismic section. Figure-12(c) shows the 3D Euler cross section of line A and Figure-12(d) shows the interpreted Euler section. The sources of anomalies were joined in the Euler section to produce lines resembling many faults numbered as 1 to 16. Basically faults interpreted from the 3D Euler cross section of line A consisting of 2 major faults and 14 minor ones separated by 7 basements in between the faults as indicated by B1-B7. Depth of faults observed in line A range from 1 to 5 km and the deepest basement depth was located at about 4 km. The shallower basement top was also clearly observed at about 2 km towards the north of the line. Similar fault patterns were also found in lines B and C where numerous normal faults forming horst and graben structures were observed. Basement high separated by deep faults were observed in all these 3 cross sections. Figure-13 shows the seismic line and the Euler section with their interpreted geological sections for line B. In general both techniques discovered the major horst and graben features along the traversing line. The horst structure with several half-grabens is clearly observed in the north and south of the interpreted seismic section (Figure-13b). Depth to the top of horst is about 2.6km and its length is about 5km with only four half-grabens are detected in the seismic section. As for the Euler result, numerous points representing the source of magnetic anomalies are shown in Figure-13(c) at depth of about 1-6 km along 20km distance. These points are joint and interpreted to be representing faults and basements along the line. A total of 25 normal faults represented by almost vertical lines steeply dipping towards the north and south and 5 basements represented by short horizontal lines are as shown in Figure-13d. Basically, both techniques managed to reveal the presence of horst structure along line B but its shape from both results are not similar. The length of the horst in seismic is about 5km and it appeared to be a flat surface while the horst from Euler appeared to be like a hill with a sharp top and shorter in length compared to length observed in seismic section. Depths of faults observed in seismic section are only about 1-2km while the faults length interpreted from Euler calculation are from 1-4km. The difference in both findings is due to its different in the source of anomaly. Seismic section is based on the elasticity of subsurface materials while the

strength of its magnetic susceptibility will determine the magnetic survey results. More iron-based materials in the Tertiary sediment faults and basement rock will determine the sensitivity of Euler deconvolution results on the other hand, these fault filling irons are not very significant to cause elasticity difference compared to the host rock and hence difference in velocity for the structure to appear in seismic section. Figure-14(a-d) shows similar analysis carried out for neighbouring line C indicating subsurface interpretation of seismic line and Euler deconvolution. As in lines A and B, line C shows almost similar results between seismic and Euler sections regarding the presence of horst and grabens extended from lines A and B. In general the long elongated almost E-W trending of horst and graben structures were detected in these three lines. The top of horst platform is at about 2.6km depth in seismic (Figure-14b) while it appears shallower at about 2km depth as observed in Euler section. The horst appears as flat in seismic as opposed to dome shape in Euler. Many half grabens separated by faults are detected at depth lower than 2.6km as seen in the seismic section and these faults are cutting the basement rock which could hardly be detected extended into the tertiary sediment. The fault patterns obtained by Euler analysis are quite different from that of seismic where they are longer and much extended into the tertiary deposit. A total of about 18 faults with lengths of about 0.5 to 4km and steeply dipping towards the north and south were observed in line C. A total of about 7 (B1-B7) Basement rocks are found at depth ranging from 2-4km.

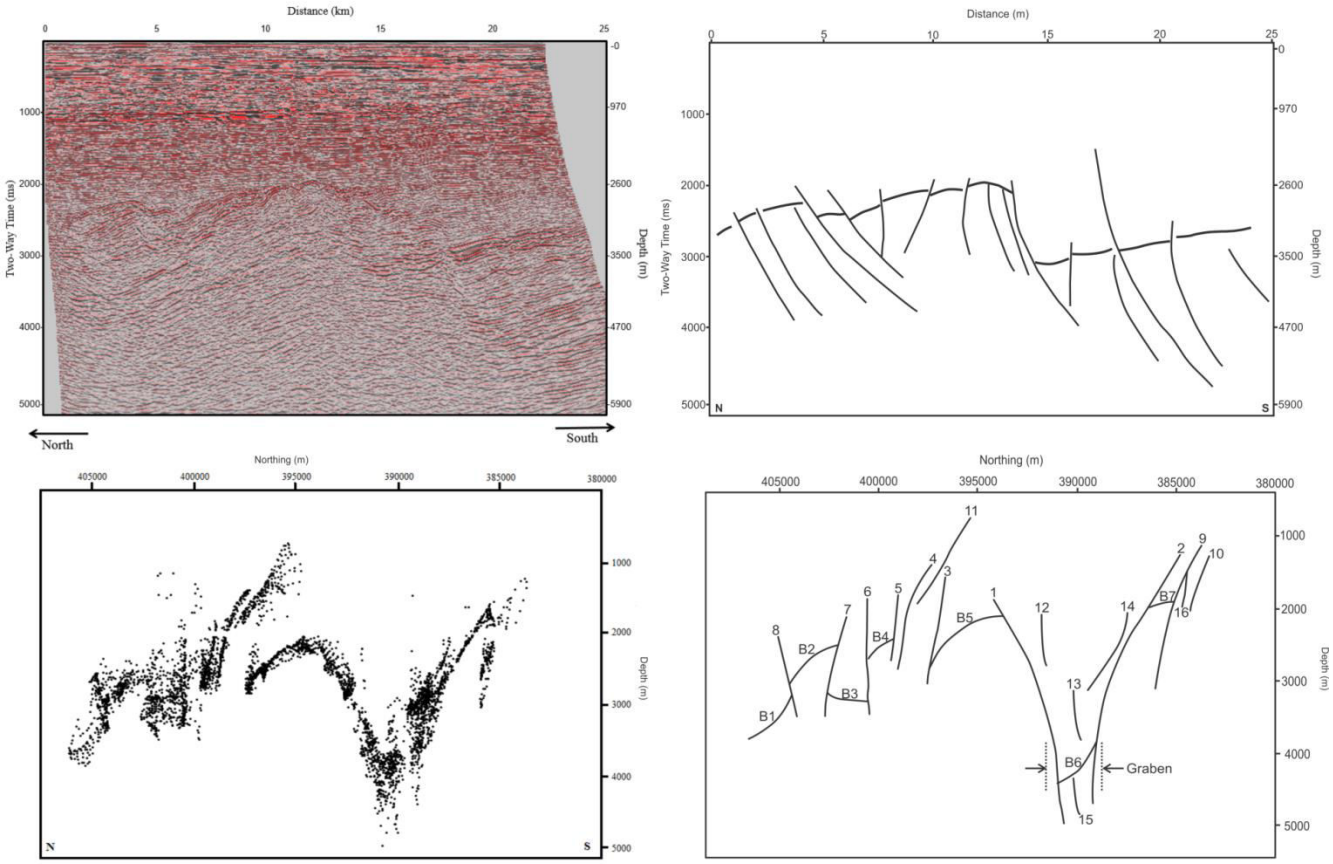

Figure-12. Seismic and Euler cross sections of line A together with its interpreted fault patterns for comparison.

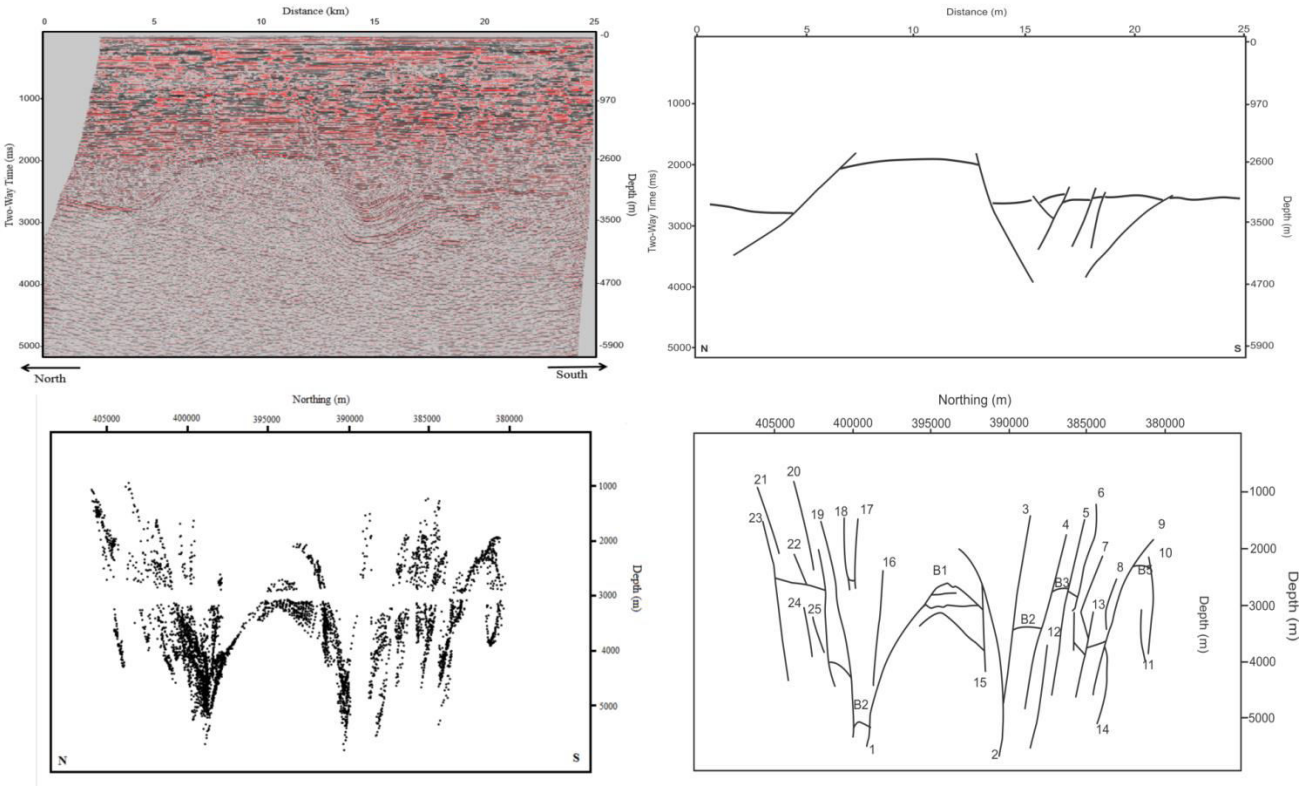

Figure-13. Seismic and Euler cross sections of line B with their interpreted fault patterns.

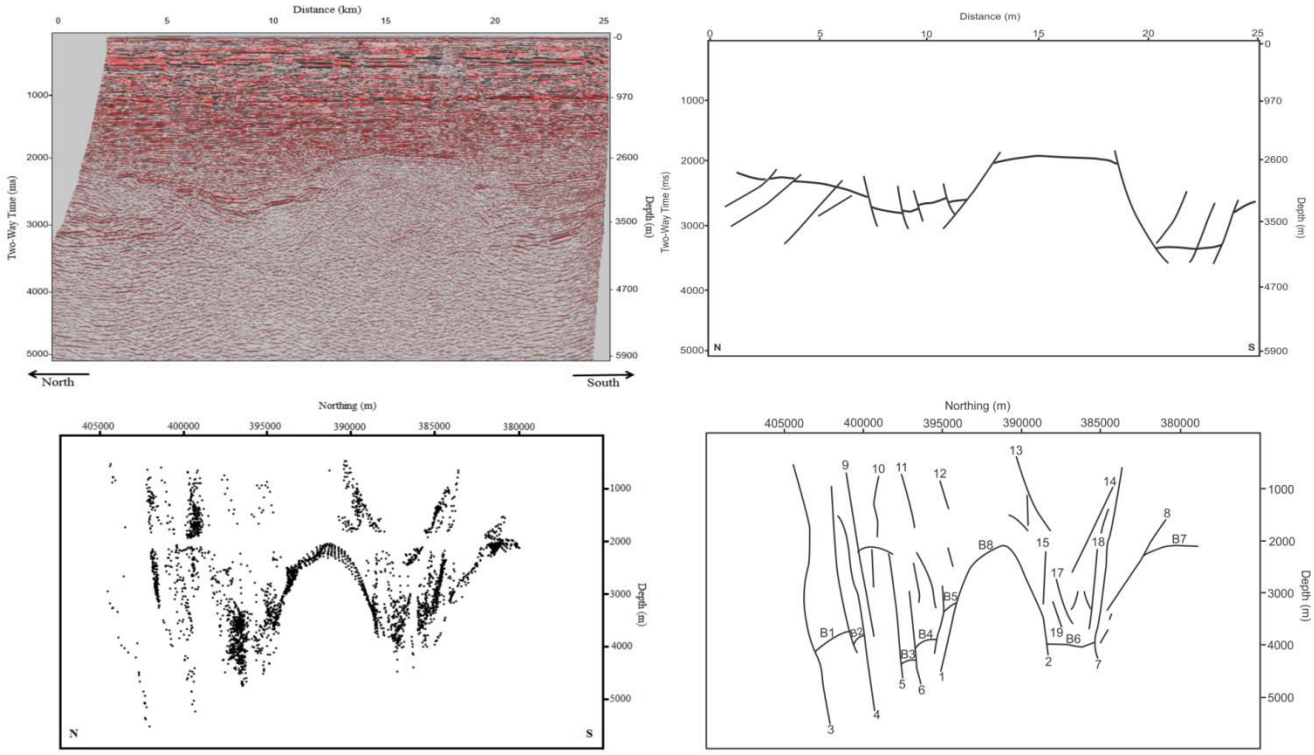

Figure-14. Seismic and Euler cross sections of line C with their interpreted fault patterns.

In general, most of the major normal fault positions obtained by Euler deconvolution were matched with faults delineated in the seismic sections especially in the basement high zone. Basically it can be concluded that Euler depth points matched quite well with the boundary of Tertiary-basement rock especially in the region of Pahang platform. Many normal faults are also shown as cutting the lower Tertiary sediments extending into the top

of basement forming half-grabens and horsts. Depths of major faults in seismic section and Euler cross section are comparable and estimated within 1500m to 4000m below the surface.

4. CONCLUSIONS

Potential field data were successfully used to estimate the structural patterns and basement depths of Penyu basin. The presence of many half grabens separated by normal faults at the base of tertiary sediment overlying the basement is confirmed by 3D Euler deconvolution analysis. Faults were clearly observed in seismic section cutting the basement but their extension into the sedimentary deposit could hardly be traced in the seismic section. Faults bordering the horst and graben structures in the tertiary sediment and basement were detected by Euler deconvolution analysis of magnetic data.

REFERENCES

Almadar, K., Ansari, A.H. and Ghorbani, A. 2009. Application of derivatives-based filters to enhance potential field features. EGU General Assembly 11, EGU2009-4071-1.

Arisoy M.O. and Dikmen U. 2015. Edge enhancement of magnetic data using fractional-order-derivative filters. Geophysics 80(1):7-17.

Cooper G.R.J. 2014. The automatic determination of the location, depth, and dip of contactsfrom aeromagnetic data.Geophysics 79(3):35-41.

Cordell, L., 1979. Gravimetric expression of graben faulting in santa Fe country and the Espanola basin, New Mexico: Guidebo. 30th Filed Conf,. Santa Fe country, N. Mex. Geological Society: 59-64.

Floria G., Fedi M. and Pasteka R. 2014. On the estimation of the structural index from low-pass filtered magnetic data.Geophysics 79(6):67-80.

Fowler C.M.R. 2005. The Solid Earth: An Introduction to Global Geophysics. United Kingdom: Cambridge University Press.

Hassan H. H., Robert A. C. and John W. P. 2015. Mapping depth to basement using 2D Werner Inversion of high-resolution aeromagnetic (HRAM) data. Extended abstract CSPG CSEG GeoConvention, Canada.

Hutchison S. E. 1989. Geological Evoluation of SE Asia. Oxford Monograph on Geology and Geophysics 13. Oxford: Clarendon Press.

Kivior I., Patricia de Lugao., Markham S., Button J., beavers S., Wise T. and Senderowitz S. 2013. Mapping basement and Moho along Equatorial Margin of Brazil using potential field data to assist petroleum exploration.

MazlanMadon AzlinaAnuar and Robert Wong. 1997. Structural evolution, maturation history and hydrocarbon potential of the Penyu Basin, offshore Peninsular Malaysia. Proceedings of an International Conference on Petroleum System of SE Asia and Australasia. 403-324.

Mazlan Madon. 1995. Tectonic evolution of Malay and Penyu basins, offshore Peninsular Malaysia. D. Phil. Thesis, University of Oxford: 355.

Ngah K., Madon M. and Tija H.D. 1996. Role off pre-tertiary fractures in formation and development of Malay and Penyu basins. Geological Society Special Publication. 106: 281-289.

Opara A.I., Embarga T.T., Oparaku O.I., Essien A.G., Onyewuchi R.A., Echetama H.N., Muze N.E. and Onwe R.M. 2015. Magnetic basement depth revaluation of Naraguta and environs north central Nigeria usisng 3D Euler deconvolution. Americal Journal ofmining and metallurgy. 3(2): 29-42.

Packham G. H. 1993. Plate tectonics and the development of sedimentary basins of the dextral regime in western Southeast Asia. Journal of Southeast Asian Earth Sciences. 1-4(8): 497-511.

Reid B., Allsop J.M., Granser H., Millet A.J. and Somerton I. W. 1990. Magneticinterpretation in three dimensions using Euler deconvolution. Geophysics. 55(1): 80-91.

Reid A. B. 1995. Euler deconvolution: Past, present and future, a review: 65th Ann. Internat. Mtg., Soc. Expl. Geophys. Expanded Abstracts, 272-273.

Reid A. B., Ebbing J. and Webb S. J. 2012. Egregious Euler Errors - the abuse of euler deconvolution applied to potential fields. 74th EAGE Conference and Exhibition incorporating SPE EUROPEC. 1-5.

Salem A., Ushijima K., Elsirafi A. and Mizunaga H. 2000. Spectral analysis of aeromagneticdata for Geothermal reconnaissance of Uaseir area, Northern Red Sea, Egypt. Proceedings of World Geothermal Congress, Kyushu-Tohokie, Japan. 28: 10.

Santos M.L., Li Y. and Moraes R. 2015. Application of 3D magnetic amplitude inversion to iron oxide-copper-gold deposits at low magnetic latitudes: A case study from Carajás Mineral Province, Brazil. Geophysics. 80(2): 13-22.

Sun Y., Yang W., Zeng X. and Zhang Z. Edge enhancement of potential field data usingspectral moments. 2016. Geophysics. 81(1): 1-11.

Tjia H. D. and Liew K. K. 1996. Changes in tectonic stress field in northern Sunda Shelf basins. Geological Society. 106: 291-306.

Waswa A., Nyamai C., Mathu E. and Ichang'i D. 2015. Application of Magnetic Survey in the Investigation of Iron Ore Deposits and Shear Zone Delineation: Case Study of Mutomo-Ikutha Area, SE Kenya. International Journal of Geosciences. 6: 729-740.

Wu P. P. C. 2004. Laboratory 4: Filtering and Euler Deconvolution of Magnetic Data. Gravity and Magnetic: GOPH 547.

Wu Q.F., Lu F. X. and L Q.S. 2003. Achaean relic body at lower crust in Sulu area: evidence from magnetic data. Chinese Science Bulletin. 48: 589-593.